Changing the interaction of a single-molecule magnetic moment with a superconductor

Stefan Schulte, Nicolas Néel, Levente Rózsa, Krisztián Palotás, and Jörg Kröger*

E-mail: joerg.kroeger@tu-ilmenau.de

Abstract

The exchange interaction of a brominated Co-porphyrin molecule with the Cooper pair condensate of Pb(111) is modified by reducing the Co–surface separation. The stepwise dehalogenation and dephenylation changes the Co adsorption height by a few picometers. Only the residual Co-porphine core exhibits a Yu-Shiba-Rusinov bound state with low binding energy in the Bardeen-Cooper-Schrieffer energy gap. Accompanying density functional calculations reveal that the Co d_{z^2}-orbital carries the molecular magnetic moment and is responsible for the intragap state. The calculated spatial evolution of the Yu-Shiba-Rusinov wave function is compatible with the experimentally observed oscillatory attenuation of the electron-hole asymmetry with increasing lateral distance from the magnetic porphine center.

Keywords: Scanning tunneling microscopy and spectroscopy, Yu-Shiba-Rusinov bound state, single-molecule chemical reaction, magnetic exchange interaction, superconductivity, density functional theory

The atomic-scale competition between superconductivity and magnetism is reflected by Yu-Shiba-Rusinov (YSR) states induced by the exchange coupling of the atomic or molecular magnetic moment with the Cooper pair condensate.[1–3] The YSR bound states appear with binding energies inside the Bardeen-Cooper-Schrieffer (BCS) energy gap of the superconductor density of states (DOS). They were reported from early planar tunneling experiments[4,5] and later from single-atom scanning tunneling spectroscopy (STS) of the differential conductance ($\mathrm{d}I/\mathrm{d}V$, I: current, V: voltage) with a scanning tunneling microscope (STM).[6] The use of superconducting tips in STS boosts the energy resolution beyond the Fermi-Dirac temperature limitation and unveils the YSR levels as clearly resolved resonance pairs within the BCS energy gap.[7] A seminal work on the competition between Kondo screening and the occurrence of YSR levels[8] stimulated renewed interest in the bound states. A good part of the ensuing research activities are presented in an excellent review article.[9]

The importance of YSR resonances is manifold. They are useful for the understanding of pairing symmetries in superconducting phases,[10–13] for recognizing topological end

modes,[14–25] for elucidating quasiparticle and Cooper pair transport across magnet–superconductor junctions[26–30] and as subtle probes for magnetic properties and interactions,[31,32] such as for the axial anisotropy of single molecules,[33] the dependence of the exchange interaction on the molecular configuration[34] or the emergence of spin moments of otherwise diamagnetic molecules in a molecular environment.[35] By the spectroscopy of YSR states, the findings of the work presented here unveil the evolution of the exchange interaction between a molecular magnetic moment and the Cooper pair condensate of an *s*-wave superconductor upon chemical modification of the molecule with the STM. The porphyrin molecule 5, 10, 15, 20-tetrakis(4-bromophenyl)-porphyrin-cobalt (TBrPPCo) undergoes the sequential removal of all Br atoms and the stepwise detachment of all phenyl groups. Only the remaining PPCo molecule exhibits a noticeable exchange interaction with the Cooper pairs of Pb(111), which is evidenced by a YSR state in $\mathrm{d}I/\mathrm{d}V$ spectroscopy. The weakness of the interaction is reflected by the low binding energy of the YSR resonance pair and the absence of the Kondo effect of PPCo. Spectroscopies of molecular orbitals and supporting calculations evidence the importance of a Co d_{z^2}-orbital and its proximity to the superconductor surface for the occurrence of the bound states. Moreover, by spatially resolved spectroscopy an oscillatory behavior of the electron-hole asymmetry is observed whose period evidences the coupling of the PPCo magnetic moment to the Pb(111) Fermi surface.

As shown in Figure 1a, the room temperature deposition of TBrPPCo on Pb(111) leads to single-layer aggregates with a nearly square unit cell spanned by the Co centers with mutual distances of $|\mathbf{a}_1| = 1.58\,\mathrm{nm}$ and $|\mathbf{a}_2| = 1.59\,\mathrm{nm}$. The molecular superstructure is incommensurate with the Pb(111) lattice and neither lattice vector $\mathbf{a}_1$ nor $\mathbf{a}_2$ is oriented along crystallographic directions of the surface ($\langle 1\bar{1}0\rangle$ is indicated by the white arrow in Figure 1a). Previously, two conformational isomers with planar and buckled adsorption geometry on Cu(111)[36] and Ag(111)[37] were reported after deposition at temperatures $<$ 100 K. Deposition at room temperature in the present work gives rise to the planar species only.

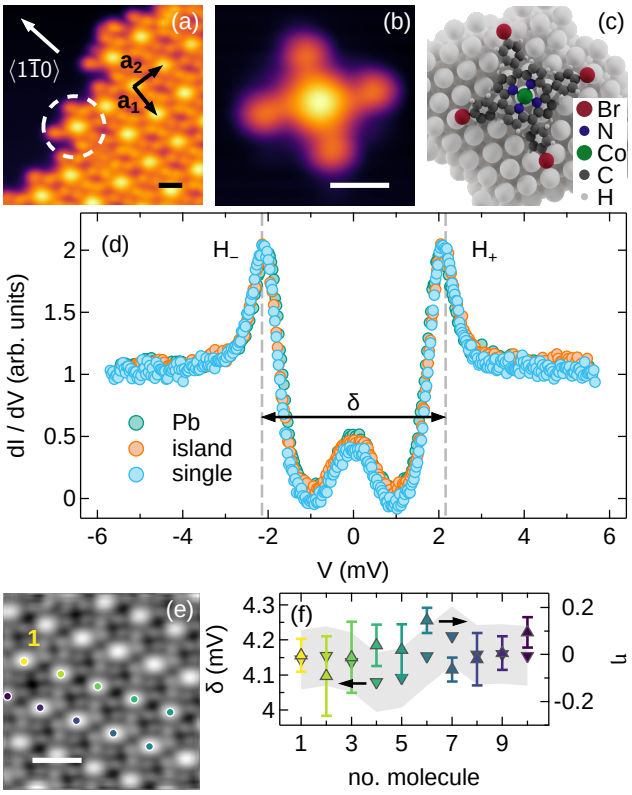

Figure 1: Adsorption of TBrPPCo on Pb(111) and spectroscopy of the BCS energy gap. (a) STM image of a TBrPPCo molecular island on Pb(111) with central Co atoms appearing brightest (bias voltage: 100 mV, tunneling current: 50 pA, scale bar: 1 nm). The superstructure is spanned by $\mathbf{a}_1$ and $\mathbf{a}_2$. A single molecule at the island edge is indicated by the dashed circle. The white arrow marks a $\langle 1\bar{1}0 \rangle$ direction. (b) STM image of an isolated TBrPPCo molecule (100 mV, 50 pA, scale bar: 1 nm). (c) Calculated relaxed adsorption geometry of TBrPPCo on Pb(111). (d) Spectra of $\mathrm{d}I/\mathrm{d}V$ acquired with a superconducting Pb tip above clean Pb(111) and atop the Co atom center of TBrPPCo embedded in an island and isolated on a substrate terrace (feedback loop parameters: 10 mV, 50 pA). H_+, H_- denote heights of spectral peaks associated with tunneling due to aligned condensation peaks of tip and sample BCS DOS; δ marks the energy gap width defined by the condensation peak distance. (e) STM image of a TBrPPCo island (100 mV, 50 pA, scale bar: 2 nm) with indicated spectroscopy sites. (f) Width δ (reversed triangles) and asymmetry η (triangles) obtained from $\mathrm{d}I/\mathrm{d}V$ spectra atop the ten molecules marked in (e). The shaded area depicts the uncertainty margin for δ.

For the desired single-molecule chemical modifications, individual molecules well separated from molecular islands were needed. To this end, molecules at island kinks (dashed circle in Figure 1a) were dragged several nm away from the island to defect-free sites on a Pb(111) terrace. Such separated TBrPPCo molecules exhibit a crosslike shape (Figure 1b) that is expected from the calculated relaxed adsorption geometry (Figure 1c). The submolecular structural motifs are assigned to the Co atom (central circular protrusion) and the four Br atoms (peripheral circular protrusions). Cross-sectional profiles along the two Br–Co–Br axes show different lengths, 1.67 nm ($\parallel \langle 1\bar{1}0\rangle$) and 1.88 nm ($\perp \langle 1\bar{1}0\rangle$). In agreement with previous structure suggestions[37,38] and the calculated relaxed adsorption geometry the Co atom resides at an on-top Pb(111) lattice site while the Br atoms prefer the proximity to hollow sites. The latter may readily be adopted by the Br atoms at the ends of a molecular axis oriented perpendicular to $\langle 1\bar{1}0\rangle$, while the other axis must bend by $\approx 4^\circ$ with respect to $\langle 1\bar{1}0\rangle$ in order to allow the Br atoms of this axis to reside at hollow sites as well. The resulting compression of TBrPPCo along this tilted direction is then in good agreement with the measured reduced length.

To probe a possible magnetic exchange coupling of the molecule to the superconductor, $\mathrm{d}I/\mathrm{d}V$ spectroscopy was performed atop the Co atom. Spectroscopy of the separated molecule as well as of TBrPPCo embedded in an island resulted in data that are not distinguishable from spectra of the clean surface (Figure 1d). In particular, gap width δ – defined as the distance between the condensation peaks (dashed lines in Figure 1d) – and electron-hole asymmetry η – defined as $\eta \equiv (H^+ - H^-)/(H^+ + H^-)$ with $H^\pm$ the condensation peak heights at positive and negative bias voltage – are the same within the uncertainty margins. The zero-bias feature visible in all spectra is due to thermally induced quasiparticle tunneling, as inferred from the good quantitative agreement between experimental data and simulations that take the finite tip and sample temperature (5 K) into account (Supporting Information). The apparent absence of YSR levels hints at an essentially vanishing magnetic exchange interaction between TBrPPCo and Pb(111). In vacuum, TBrPPCo possesses

a magnetic moment of 1.08 μ_B (μ_B: Bohr magneton), which is assigned to the partially occupied Co $3d^7$-levels.[38] The first-principle calculations used here (Supporting Information) give rise to a magnetic moment of 0.96 μ_B of the adsorbed molecule. This reduction of the molecular magnetic moment is likely due to charge transfer from the surface, as likewise reported for TBrPPCo on Cu(111).[36] Spectral data acquired across the molecule, i. e., away from the Co center, are likewise virtually identical with data recorded atop clean Pb(111). In order to explore a possible impact of the adsorption site, dI/dV data were acquired atop TBrPPCo molecules embedded in an island (Figure 1e). For the ten indicated molecules that adopt slightly different adsorption sites owing to the incommensurate molecular superstructure, Figure 1f summarizes the extracted values for δ and η with no identifiable effect.

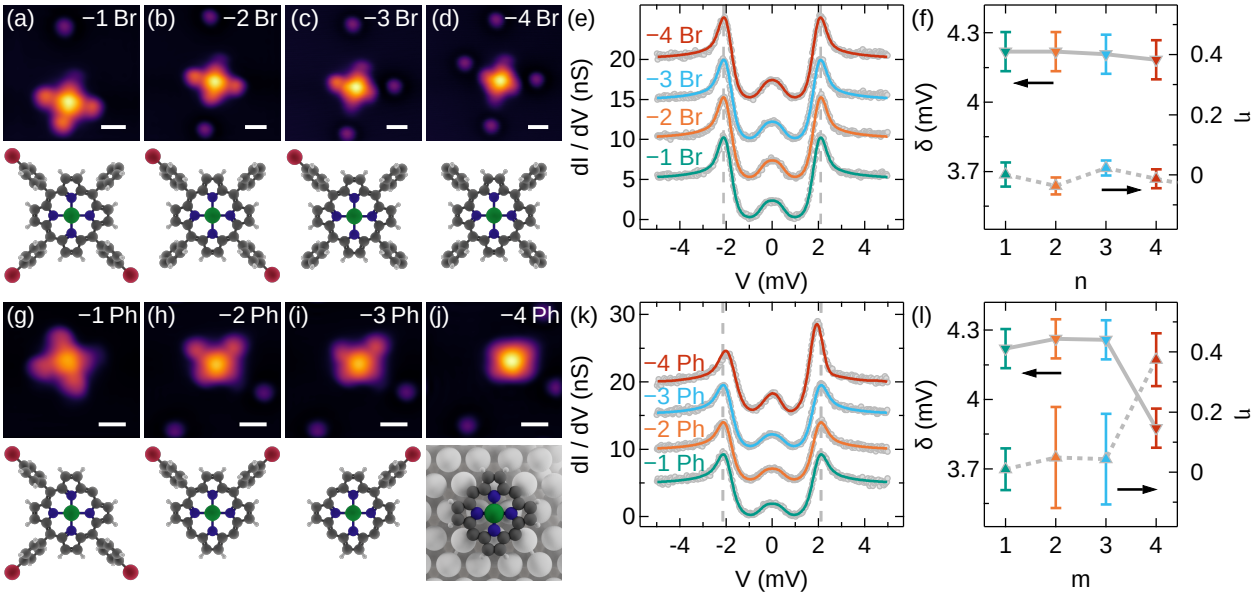

Figure 2: Stepwise dehalogenation and dephenylation of TBrPPCo together with low-voltage spectral data. (a)–(d) STM images of atomwise dehalogenated molecules $-n$ Br ($n = 1 \ldots 4$) (100 mV, 50 pA, scale bar: 1 nm). (e) dI/dV spectra (dots) of $-n$ Br acquired atop the central Co atom. Spectra of $-n$ Br ($n = 2 \ldots 4$) are vertically offset. Solid lines represent fits to the data (Supporting Information). (f) δ (reversed triangles) and η (triangles) as a function of n. (g)–(j) As (a)–(d) for stepwise dephenylated molecules $-m$ Ph ($m = 1 \ldots 4$). In (j) the calculated relaxed adsorption geometry of -4 Ph is presented. (k), (l) As (e), (f) for $-m$ Ph.

In the next step of the experiments, individual Br atoms and phenyl moieties were detached (Supporting Information) to explore a possible effect on the magnetic interaction with

Pb(111). To this end, the peripheral Br atoms were abstracted atom by atom (Figure 2a–d). For each product molecule, referred to as $-n\,\mathrm{Br}$ with $n = 1 \ldots 4$, a $\mathrm{d}I/\mathrm{d}V$ spectrum was acquired atop the Co center (Figure 2e). Both δ and η (Figure 2f) are similar to observations from intact TBrPPCo for all $-n\,\mathrm{Br}$, indicating a similarly weak magnetic exchange coupling of $-n\,\mathrm{Br}$ molecules to Pb(111) Cooper pairs as for TBrPPCo.

The TBrPPCo molecule was also dephenylated step by step leading to molecular products denoted by $-m\,\mathrm{Ph}$ ($m = 1 \ldots 4$) (Figure 2g–j). Marked changes in $\mathrm{d}I/\mathrm{d}V$ spectra occur only for $m = 4$ (top spectrum of Figure 2k). The gap width δ decreases and the peaks at the gap edges adopt asymmetric heights. These modifications are assigned to the occurrence of YSR resonances inside the BCS energy gap. In order to determine the binding energy and electron-hole asymmetry of the YSR levels, spectral data were fit by considering temperature and modulation broadening and by convolution of the tip with the sample DOS (Supporting Information). The obtained binding energy of the single YSR state is $\varepsilon = 1.18\,\mathrm{meV}$, which is very close to the BCS order parameter of the sample $\Delta_\mathrm{s} = 1.31\,\mathrm{meV}$ at the sample temperature $T_\mathrm{s} = 4.8\,\mathrm{K}$. This observation together with the higher resonance strength at positive bias voltage supports the idea of a low magnetic exchange coupling between $-4\,\mathrm{Ph}$ and Pb(111), as well as of $-4\,\mathrm{Ph}$ representing a spin $S = 1/2$ magnetic impurity. Calculations (Supporting Information) unveil a $-4\,\mathrm{Ph}$ magnetic moment of $1.02\,\mu_\mathrm{B}$, similar to the moment for intact TBrPPCo, which corroborates the treatment of the molecules as a magnetic impurity with spin $S = 1/2$. Therefore, the occurrence of YSR resonances for $-4\,\mathrm{Ph}$ can be attributed to the enhanced hybridization between the Co d-orbitals and the substrate, which in turn increase the exchange coupling compared to intact TBrPPCo. This conclusion matches the bridge adsorption site of Co in $-4\,\mathrm{Ph}$ (Figure 2j), which is coordinated by two Pb atoms rather than one for the on-top site of Co in the intact molecule. Moreover, the calculated Co vertical distance to the surface is 8 pm lower for PPCo than observed from TBrPPCo (Supporting Information). Despite the increased hybridization between PPCo and Pb(111) the magnetic exchange interaction remains weak, which besides the low binding energy of

the YSR state is reflected by the absence of an Abrikosov-Suhl-Kondo resonance that would indicate the Kondo effect[39,40] (Supporting Information). This interpretation is in accordance with a previous work, where the Kondo effect was only observed for those magnetic transition metal atoms on Re(0001) that induced YSR states sufficiently far from the BCS energy gap edges.[41] The resulting Kondo temperature for the molecules reported here is therefore likely below the temperature accessible in the experiments.

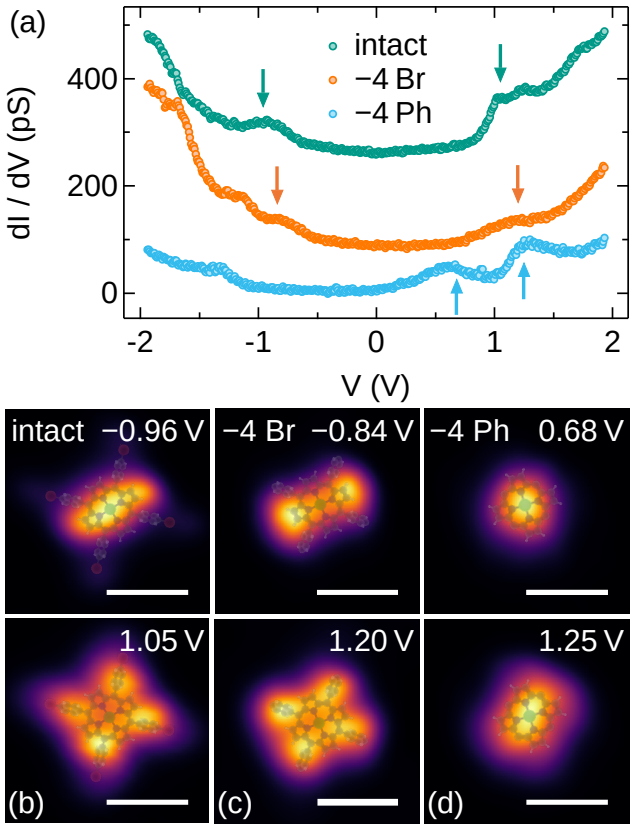

Figure 3: Orbital electronic structure of intact and manipulated molecules. (a) dI/dV spectra of indicated molecules acquired atop the central Co atom (feedback loop parameters: 1 V, 50 pA). (b)–(d) Normalized constant-current maps of dI/dV recorded at marked bias voltages (arrows in (a)) for the (b) intact, (c) fully dehalogenated and (d) entirely dephenylated molecule (50 pA, scale bar: 1 nm).

The increased hybridization of −4 Ph with Pb(111) can also be inferred from the molecular electronic structure seen in dI/dV spectroscopy covering a wider bias voltage range. Such data are presented in Figure 3a, which displays dI/dV spectra acquired atop the Co atom of intact TBrPPCo, −4 Br and −4 Ph. For the intact molecule, a broad peak at ≈ -0.93 V and

a steplike feature with its rising edge at $\approx 0.94\,\mathrm{V}$ are assigned to the highest occupied molecular orbital (HOMO) and the lowest unoccupied molecular orbital (LUMO), respectively. After removal of 4 Br atoms, the original HOMO signature is split into two steplike features with rising edges at $\approx -1.07\,\mathrm{V}$ and $\approx -0.66\,\mathrm{V}$, while the LUMO spectroscopic signal occurs at a similar voltage as observed for the intact molecule and is strongly attenuated. The region of spectral data between the HOMO and LUMO of $-4\,\mathrm{Br}$ remains depleted, similar to TBrPPCo. Stronger modifications of the spectral data are observed for $-4\,\mathrm{Ph}$ where the HOMO signal nearly disappeared and the LUMO-associated feature turned into an enhanced peak at $\approx 1.28\,\mathrm{V}$. In addition, a peak occurs at $\approx 0.61\,\mathrm{V}$ with a tail straddling $0\,\mathrm{V}$.

To further characterize these spectral signatures, spatial maps of $\mathrm{d}I/\mathrm{d}V$ were acquired close to the aforementioned characteristic voltages (Figure 3b–d). In order to ensure a good approximation of the constant-current $\mathrm{d}I/\mathrm{d}V$ map to the spatial variation of the sample DOS, map data were normalized.[42] The most important conclusion from these maps is the spatial localization of the spectroscopic feature at $0.61\,\mathrm{V}$ to the Co site, which is indicative of a d_{z^2}-orbital character. Combining this assignment with the observed zero-bias straddling of the orbital spectroscopic signature, which correspond to the overlap of the orbital with the Fermi energy, lends support to the idea that the Co d_{z^2}-orbital is mainly involved in the magnetic exchange interaction with the Cooper pairs and, thus, in inducing the YSR state. The calculations confirm that the singly occupied d_{z^2}-orbital gives rise to the Co magnetic moment.

After identifying the molecular orbital inducing the YSR bound states, the coupling of the magnetic impurity to the Fermi surface of the two-band superconductor Pb(111)[43,44] remains to be explored. The spatial evolution of $\mathrm{d}I/\mathrm{d}V$ spectra with increasing distance r from the Co center of $-4\,\mathrm{Ph}$ was measured along $\langle 1\bar{1}0\rangle$ (Figure 4a) and along a direction deviating from $\langle 1\bar{1}0\rangle$ (Figure 4b). The extracted spatially resolved asymmetry, $\eta(r)$, is shown in Figure 4c,d. Along $\langle 1\bar{1}0\rangle$ (Figure 4c) a clear oscillatory behavior of η is observed at a finite distance from the Co atom, while it is less pronounced for directions off $\langle 1\bar{1}0\rangle$ (Figure

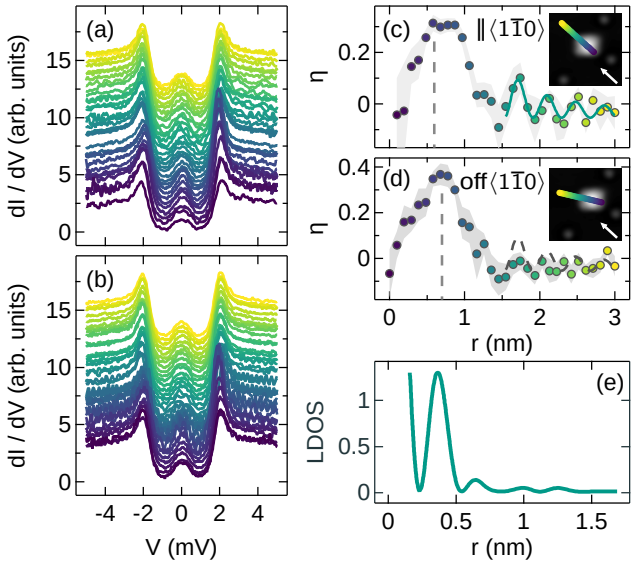

Figure 4: Experimental spatial evolution of electron-hole asymmetry and comparison with calculated DOS. (a) Series of $\mathrm{d}I/\mathrm{d}V$ spectra acquired along $\langle 1\bar{1}0\rangle$ across -4 Ph. (b) As (a) for a direction off $\langle 1\bar{1}0\rangle$. Feedback loop parameters for spectra in (a),(b): 10 mV, 50 pA. (c) Spatial evolution of η (dots) with Co center at $r = 0.6$ nm (vertical dashed line). The solid line is a fit to the data according to eq 1. (d) As (c) for an off-$\langle 1\bar{1}0\rangle$ direction with the Co atom at $r = 0.7$ nm. The dashed undulating line is the same as the solid line in (c) for comparison. Insets to (c),(d): STM images of -4 Ph with marked spectroscopy sites (100 mV, 50 pA, 4.5 nm $\times$ 4.5 nm). The arrow indicates a $\langle 1\bar{1}0\rangle$ direction. (e) Calculated local DOS spatial variation with the Co atom located at $r = 0$.

4d). The more pronounced oscillatory decay along $\langle 1\bar{1}0\rangle$ is most likely due to an electron-focusing effect, which occurs for directions normal to flat Fermi surface contours. In this case, many parallel scattering vectors spanning the flat contours are accumulated, giving rise to a spatially extended scattering pattern. This interpretation is in agreement with similar observations from buried Co atoms at Cu(111),[45] Ne atoms at Pb(100),[44] magnetic impurities (Fe, Nd, Ni) at La(0001)[46] as well as from Mn atoms adsorbed on Pb(111)[47] and recent simulations for arbitrary Fermi surfaces contours.[48,49] For an isotropic Fermi surface and a pointlike magnetic impurity at r_0, the spatial evolution of the YSR state follows an oscillatory decay given by

$$|\psi_{\pm}(r)|^2 \propto \frac{\sin^2[k_{\mathrm{F}}(r-r_0)+\delta^{\pm}]}{[k_{\mathrm{F}}(r-r_0)]^{d-1}} \cdot \exp\left[-2|\sin(\delta^{+}-\delta^{-})|\frac{r-r_0}{\xi}\right] \qquad (1)$$

with $\pm$ denoting the electron (+) and hole (−) component of the wave function ψ, k_{F} the Fermi wave vector, $\delta^{\pm}$ the scattering phase shift, d the dimensionality of the scattering and ξ the BCS coherence length.[11,47,50] For the fit (solid line in Figure 4c) of experimental data by the expression in eq 1, $\delta^{+}-\delta^{-}\approx 0$ is assumed. This is a reasonable assumption because the YSR energy $\varepsilon = \Delta_{\mathrm{s}}\cdot\cos(\delta^{+}-\delta^{-})$ (Ref. 11) is close to Δ_{s}. Consequently, the exponential term in eq 1 is nearly unity and it is thus difficult to extract information on ξ. The fit gives rise to $d = 2$, which is in agreement with the calculated spatial decay (Figure 4e) and indicates that surface effects dominate. Remarkably, $k_{\mathrm{F}} = (8.23 \pm 0.33)\,\mathrm{nm}^{-1}$ as determined from the fit leads to a Fermi wavelength $\lambda_{\mathrm{F}} = (723 \pm 31)\,\mathrm{pm}$, which is significantly shorter than the Fermi wavelength of $\lambda_{\mathrm{F}} = 1160\,\mathrm{pm}$ reported previously for YSR states induced by a Mn atom on Pb(111).[47] The Fermi surface of Pb consists of a rounded octahedron with Fermi wavelengths in the range of $\lambda_{\mathrm{F}}^{(1)} = 800$–$900\,\mathrm{pm}$ and a netlike structure enclosing the edges of the Brillouin zone with $\lambda_{\mathrm{F}}^{(2)} = 500$–$600\,\mathrm{pm}$. The two sheets of the Fermi surface reflect the two-band superconducting nature of Pb.[43,44] The Fermi wavelength determined from the present fit is in reasonable agreement with $\lambda_{\mathrm{F}}^{(1)}$, the inner Fermi surface displaying a combination of

s, p and d electronic character. The complex Fermi surface of Pb and the difference in the oscillation periods between the present and previous[47] work indicate that using eq 1 with a k_F independent of the magnetic scatterer is too crude an approximation. Simulations taking into account the complete electronic structure of Pb(111) as well as the spatial profile of the scattering potential due to the d_{z^2}-orbital of Co extracted from first-principles calculations resulted in an oscillation period that is consistent with a Fermi wavelength of 700 pm (Figure 4e), in reasonable agreement with the experimental observations.

In conclusion, YSR resonances act as subtle probes for the magnetic exchange interaction between an atomic or molecular magnetic moment with the Cooper pair condensate of a superconductor. By controllable removal of molecular moieties of TBrPPCo on Pb(111) the magnetic exchange coupling was increased owing to the gradually raised Co–surface hybridization. The entirely dehalogenated and dephenylated residual PPCo molecule induced a single YSR state in the superconductor energy gap. The underlying exchange coupling is mediated by the Co d_{z^2}-orbital, which straddles the Fermi level evidencing its hybridization with the substrate electronic structure. The spatial oscillation of the electron-hole asymmetry demonstrates the presence of a magnetic scattering potential. For accurately describing YSR states, the complex Fermi surface of the superconductor and the spatial profile of the scattering potential must be considered.

Experimental method. The STM/STS experiments were performed at low temperature (4.8 K) and in ultrahigh vacuum (10^{-9} Pa). Surfaces of Pb(111) were prepared by Ar^+ bombardment (partial pressure, 10^{-4} Pa; ion kinetic energy, 1.2 keV; target current, 10 μA) and annealing (570 K). Highly purified (99.9 %) TBrPPCo powder was sublimated from a heated (610 K) Ta crucible and deposited on clean Pb(111) at room temperature. Pure (99.95 %) W wire (diameter, 0.25 mm) was chemically etched in 0.1 M NaOH and used as the tip material, which was further treated in situ by field emission on a Au target. Superconducting tips were obtained by coating the tip apex with substrate material in the course of repeated indentations into Pb(111) and optimizing the tip apex by single-atom transfer

from the tip to the surface.[51–56] Images were acquired in constant-current mode with the bias voltage applied to the sample. Spectroscopy of $\mathrm{d}I/\mathrm{d}V$ proceeded via the sinusoidal modulation ($100\,\mu\mathrm{V_{rms}}$, 713 Hz) of the bias voltage and recording the first harmonic of the resulting ac current across the tunneling barrier with a lock-in amplifier.

Theoretical method. Density functional calculations were performed using the Vienna Ab-initio Simulation Package[57,58] with projector augmented waves[59] and van der Waals correction at the optB86b level.[60,61] For describing the YSR states, a previously reported theoretical approach[62] was used. More details are found in the Supporting Information.

Acknowledgement

Funding by the Deutsche Forschungsgemeinschaft (Grant No. KR 2912/18-1), the German Federal Ministry of Education and Research within the "Forschungslabore Mikroelektronik Deutschland (ForLab)" initiative, the János Bolyai Research Grant of the Hungarian Academy of Sciences (Grant No. BO/292/21/11), the National Research Development and Innovation (NRDI) Office of Hungary under projects No. FK124100 and No. K131938, the New National Excellence Program of the Ministry for Culture and Innovation from NRDI Fund (Grant No. ÚNKP-22-5-BME-282) and the Young Scholar Fund at the University of Konstanz as well as discussion with Stefan Kirchner are acknowledged.

Supporting Information Available

The Supporting Information is available free of charge on the ACS Publications website at DOI: [hyperlink DOI]

Fit algorithm; Single-porphyrin modifications; Absence of the Kondo effect; Density functional calculation details of the molecular adsorption; Modeling of the Yu-Shiba-Rusinov states

Corresponding Author

Jörg Kröger — Institut für Physik, Technische Universität Ilmenau, D-98693 Ilmenau, Germany; Email: joerg.kroeger@tu-ilmenau.de

Authors

Stefan Schulte — Institut für Physik, Technische Universität Ilmenau, D-98693 Ilmenau, Germany; Present address: Peter Grünberg Institut, Forschungszentrum Jülich, D-52425 Jülich, Germany and II. Physikalisches Institut, Universität zu Köln, D-50923, Germany

Nicolas Néel — Institut für Physik, Technische Universität Ilmenau, D-98693 Ilmenau, Germany

Levente Rózsa — Fachbereich Physik, Universität Konstanz, D-78457 Konstanz, Germany

Krisztián Palotás — Department of Theoretical Solid State Physics, Institute for Solid State Physics and Optics, Wigner Research Center for Physics, H-1121 Budapest, Hungary; ELKH-SZTE Reaction Kinetics and Surface Chemistry Research Group, University of Szeged, H-6720 Szeged, Hungary; Department of Theoretical Physics, Institute of Physics, Budapest University of Technology and Economics, H-1111 Budapest, Hungary

References

(1) Yu, L. Bound state in superconductors with paramagnetic impurities. *Acta Physica Sinica* **1965**, *21*, 75 – 90.

(2) Shiba, H. Classical Spins in Superconductors. *Progress of Theoretical Physics* **1968**, *40*, 435–451.

(3) Rusinov, A. I. Superconductivity near a Paramagnetic Impurity. *JETP Letters* **1969**, *9*, 85 – 87.

(4) Woolf, M. A.; Reif, F. Effect of Magnetic Impurities on the Density of States of Superconductors. *Phys. Rev.* **1965**, *137*, A557–A564.

(5) Bauriedl, W.; Ziemann, P.; Buckel, W. Electron-Tunneling Observation of Impurity Bands in Superconducting Manganese-Implanted Lead. *Phys. Rev. Lett.* **1981**, *47*, 1163–1165.

(6) Yazdani, A.; Jones, B. A.; Lutz, C. P.; Crommie, M. F.; Eigler, D. M. Probing the Local Effects of Magnetic Impurities on Superconductivity. *Science* **1997**, *275*, 1767–1770.

(7) Ji, S.-H.; Zhang, T.; Fu, Y.-S.; Chen, X.; Ma, X.-C.; Li, J.; Duan, W.-H.; Jia, J.-F.; Xue, Q.-K. High-Resolution Scanning Tunneling Spectroscopy of Magnetic Impurity Induced Bound States in the Superconducting Gap of Pb Thin Films. *Phys. Rev. Lett.* **2008**, *100*, 226801.

(8) Franke, K. J.; Schulze, G.; Pascual, J. I. Competition of Superconducting Phenomena and Kondo Screening at the Nanoscale. *Science* **2011**, *332*, 940–944.

(9) Heinrich, B. W.; Pascual, J. I.; Franke, K. J. Single magnetic adsorbates on s-wave superconductors. *Progress in Surface Science* **2018**, *93*, 1–19.

(10) Salkola, M. I.; Balatsky, A. V.; Schrieffer, J. R. Spectral properties of quasiparticle excitations induced by magnetic moments in superconductors. *Phys. Rev. B* **1997**, *55*, 12648–12661.

(11) Balatsky, A. V.; Vekhter, I.; Zhu, J.-X. Impurity-induced states in conventional and unconventional superconductors. *Rev. Mod. Phys.* **2006**, *78*, 373–433.

(12) Shindou, R.; Furusaki, A.; Nagaosa, N. Quantum impurity spin in Majorana edge fermions. *Phys. Rev. B* **2010**, *82*, 180505.

(13) Žitko, R.; Simon, P. Quantum impurity coupled to Majorana edge fermions. *Phys. Rev. B* **2011**, *84*, 195310.

(14) Klinovaja, J.; Stano, P.; Yazdani, A.; Loss, D. Topological Superconductivity and Majorana Fermions in RKKY Systems. *Phys. Rev. Lett.* **2013**, *111*, 186805.

(15) Pientka, F.; Glazman, L. I.; von Oppen, F. Topological superconducting phase in helical Shiba chains. *Phys. Rev. B* **2013**, *88*, 155420.

(16) Nadj-Perge, S.; Drozdov, I. K.; Li, J.; Chen, H.; Jeon, S.; Seo, J.; MacDonald, A. H.; Bernevig, B. A.; Yazdani, A. Observation of Majorana fermions in ferromagnetic atomic chains on a superconductor. *Science* **2014**, *346*, 602–607.

(17) Ruby, M.; Pientka, F.; Peng, Y.; von Oppen, F.; Heinrich, B. W.; Franke, K. J. End States and Subgap Structure in Proximity-Coupled Chains of Magnetic Adatoms. *Phys. Rev. Lett.* **2015**, *115*, 197204.

(18) Jeon, S.; Xie, Y.; Li, J.; Wang, Z.; Bernevig, B. A.; Yazdani, A. Distinguishing a Majorana zero mode using spin-resolved measurements. *Science* **2017**, *358*, 772–776.

(19) Feldman, B. E.; Randeria, M. T.; Li, J.; Jeon, S.; Xie, Y.; Wang, Z.; Drozdov, I. K.; Andrei Bernevig, B.; Yazdani, A. High-resolution studies of the Majorana atomic chain platform. *Nature Physics* **2016**, *13*, 286–291.

(20) Pawlak, R.; Kisiel, M.; Klinovaja, J.; Meier, T.; Kawai, S.; Glatzel, T.; Loss, D.; Meyer, E. Probing atomic structure and Majorana wavefunctions in mono-atomic Fe chains on superconducting Pb surface. *npj Quantum Information* **2016**, *2*, 16035.

(21) Ruby, M.; Heinrich, B. W.; Peng, Y.; von Oppen, F.; Franke, K. J. Exploring a Proximity-Coupled Co Chain on Pb(110) as a Possible Majorana Platform. *Nano Letters* **2017**, *17*, 4473–4477.

(22) Cornils, L.; Kamlapure, A.; Zhou, L.; Pradhan, S.; Khajetoorians, A. A.; Fransson, J.; Wiebe, J.; Wiesendanger, R. Spin-Resolved Spectroscopy of the Yu-Shiba-Rusinov States of Individual Atoms. *Phys. Rev. Lett.* **2017**, *119*, 197002.

(23) Li, J.; Jeon, S.; Xie, Y.; Yazdani, A.; Bernevig, B. A. Majorana spin in magnetic atomic chain systems. *Phys. Rev. B* **2018**, *97*, 125119.

(24) Schneider, L.; Beck, P.; Posske, T.; Crawford, D.; Mascot, E.; Rachel, S.; Wiesendanger, R.; Wiebe, J. Topological Shiba bands in artificial spin chains on superconductors. *Nature Physics* **2021**, *17*, 943 – 948.

(25) Schneider, L.; Beck, P.; Neuhaus-Steinmetz, J.; Rózsa, L.; Posske, T.; Wiebe, J.; Wiesendanger, R. Precursors of Majorana modes and their length-dependent energy oscillations probed at both ends of atomic Shiba chains. *Nature Nanotechnology* **2022**, *17*, 384 – 389.

(26) Ruby, M.; Pientka, F.; Peng, Y.; von Oppen, F.; Heinrich, B. W.; Franke, K. J. Tunneling Processes into Localized Subgap States in Superconductors. *Phys. Rev. Lett.* **2015**, *115*, 087001.

(27) Randeria, M. T.; Feldman, B. E.; Drozdov, I. K.; Yazdani, A. Scanning Josephson spectroscopy on the atomic scale. *Phys. Rev. B* **2016**, *93*, 161115.

(28) Farinacci, L.; Ahmadi, G.; Reecht, G.; Ruby, M.; Bogdanoff, N.; Peters, O.; Heinrich, B. W.; von Oppen, F.; Franke, K. J. Tuning the Coupling of an Individual Magnetic Impurity to a Superconductor: Quantum Phase Transition and Transport. *Phys. Rev. Lett.* **2018**, *121*, 196803.

(29) Brand, J.; Gozdzik, S.; Néel, N.; Lado, J. L.; Fernández-Rossier, J.; Kröger, J. Electron and Cooper-pair transport across a single magnetic molecule explored with a scanning tunneling microscope. *Phys. Rev. B* **2018**, *97*, 195429.

(30) Villas, A.; Klees, R. L.; Huang, H.; Ast, C. R.; Rastelli, G.; Belzig, W.; Cuevas, J. C. Interplay between Yu-Shiba-Rusinov states and multiple Andreev reflections. *Phys. Rev. B* **2020**, *101*, 235445.

(31) Flatté, M. E.; Reynolds, D. E. Local spectrum of a superconductor as a probe of interactions between magnetic impurities. *Phys. Rev. B* **2000**, *61*, 14810–14814.

(32) Meng, T.; Klinovaja, J.; Hoffman, S.; Simon, P.; Loss, D. Superconducting gap renormalization around two magnetic impurities: From Shiba to Andreev bound states. *Phys. Rev. B* **2015**, *92*, 064503.

(33) Heinrich, B. W.; Braun, L.; Pascual, J. I.; Franke, K. J. Tuning the Magnetic Anisotropy of Single Molecules. *Nano Letters* **2015**, *15*, 4024–4028.

(34) Malavolti, L.; Briganti, M.; Hänze, M.; Serrano, G.; Cimatti, I.; McMurtrie, G.; Otero, E.; Ohresser, P.; Totti, F.; Mannini, M.; Sessoli, R.; Loth, S. Tunable Spin–Superconductor Coupling of Spin 1/2 Vanadyl Phthalocyanine Molecules. *Nano Letters* **2018**, *18*, 7955–7961.

(35) Homberg, J.; Weismann, A.; Berndt, R.; Gruber, M. Inducing and Controlling Molecular Magnetism through Supramolecular Manipulation. *ACS Nano* **2020**, *14*, 17387–17395.

(36) Iancu, V.; Deshpande, A.; Hla, S.-W. Manipulating Kondo Temperature via Single Molecule Switching. *Nano Letters* **2006**, *6*, 820–823.

(37) Kreuch, T.; Meierott, S.; Néel, N.; Beenken, W. J. D.; Kröger, J. Atom-by-Atom Dehalogenation of a Porphyrin Molecule Adsorbed on Ag(111). *The Journal of Physical Chemistry C* **2014**, *118*, 30162–30169.

(38) Perera, U. G. E.; Kulik, H. J.; Iancu, V.; Dias da Silva, L. G. G. V.; Ulloa, S. E.; Marzari, N.; Hla, S.-W. Spatially Extended Kondo State in Magnetic Molecules Induced by Interfacial Charge Transfer. *Phys. Rev. Lett.* **2010**, *105*, 106601.

(39) Li, J.; Schneider, W.-D.; Berndt, R.; Delley, B. Kondo Scattering Observed at a Single Magnetic Impurity. *Phys. Rev. Lett.* **1998**, *80*, 2893–2896.

(40) Madhavan, V.; Chen, W.; Jamneala, T.; Crommie, M. F.; Wingreen, N. S. Tunneling into a Single Magnetic Atom: Spectroscopic Evidence of the Kondo Resonance. *Science* **1998**, *280*, 567–569.

(41) Schneider, L.; Steinbrecher, M.; Rózsa, L.; Bouaziz, J.; Palotás, K.; dos Santos Dias, M.; Lounis, S.; Wiebe, J.; Wiesendanger, R. Magnetism and in-gap states of 3d transition metal atoms on superconducting Re. *npj Quantum Materials* **2019**, *4*, 42.

(42) Ziegler, M.; Néel, N.; Sperl, A.; Kröger, J.; Berndt, R. Local density of states from constant-current tunneling spectra. *Phys. Rev. B* **2009**, *80*, 125402.

(43) Floris, A.; Sanna, A.; Massidda, S.; Gross, E. K. U. Two-band superconductivity in Pb from ab initio calculations. *Phys. Rev. B* **2007**, *75*, 054508.

(44) Ruby, M.; Heinrich, B. W.; Pascual, J. I.; Franke, K. J. Experimental Demonstration of a Two-Band Superconducting State for Lead Using Scanning Tunneling Spectroscopy. *Phys. Rev. Lett.* **2015**, *114*, 157001.

(45) Weismann, A.; Wenderoth, M.; Lounis, S.; Zahn, P.; Quaas, N.; Ulbrich, R. G.; Dederichs, P. H.; Blügel, S. Seeing the Fermi Surface in Real Space by Nanoscale Electron Focusing. *Science* **2009**, *323*, 1190–1193.

(46) Kim, H.; Rózsa, L.; Schreyer, D.; Simon, E.; Wiesendanger, R. Long-range focusing of magnetic bound states in superconducting lanthanum. *Nature Communications* **2020**, *11*, 4573.

(47) Ruby, M.; Peng, Y.; von Oppen, F.; Heinrich, B. W.; Franke, K. J. Orbital Picture of Yu-Shiba-Rusinov Multiplets. *Phys. Rev. Lett.* **2016**, *117*, 186801.

(48) Uldemolins, M.; Mesaros, A.; Simon, P. Quasiparticle focusing of bound states in two-dimensional *s*-wave superconductors. *Phys. Rev. B* **2022**, *105*, 144503.

(49) Ortuzar, J.; Trivini, S.; Alvarado, M.; Rouco, M.; Zaldivar, J.; Yeyati, A. L.; Pascual, J. I.; Bergeret, F. S. Yu-Shiba-Rusinov states in two-dimensional superconductors with arbitrary Fermi contours. *Phys. Rev. B* **2022**, *105*, 245403.

(50) Ménard, G. C.; Guissart, S.; Brun, C.; Pons, S.; Stolyarov, V. S.; Debontridder, F.; Leclerc, M. V.; Janod, E.; Cario, L.; Roditchev, D.; Simon, P.; Cren, T. Coherent long-range magnetic bound states in a superconductor. *Nature Physics* **2015**, *11*, 1013–1016.

(51) Limot, L.; Kröger, J.; Berndt, R.; Garcia-Lekue, A.; Hofer, W. A. Atom Transfer and Single-Adatom Contacts. *Phys. Rev. Lett.* **2005**, *94*, 126102.

(52) Kröger, J.; Jensen, H.; Berndt, R. Conductance of Tip–Surface and Tip–Atom Junctions on Au(111) Explored by a Scanning Tunnelling Microscope. *New J. Phys.* **2007**, *9*, 153.

(53) Kröger, J.; Néel, N.; Limot, L. Contact to Single Atoms and Molecules with the Tip of a Scanning Tunnelling Microscope. *J. Phys.: Condens. Matter* **2008**, *20*, 223001.

(54) Kröger, J.; Néel, N.; Sperl, A.; Wang, Y. F.; Berndt, R. Single-Atom Contacts with a Scanning Tunnelling Microscope. *New J. Phys.* **2009**, *11*, 125006.

(55) Berndt, R.; Kröger, J.; Néel, N.; Schull, G. Controlled Single Atom and Single Molecule Contacts. *Phys. Chem. Chem. Phys.* **2010**, *12*, 1022–1032.

(56) Müller, M.; Salgado, C.; Néel, N.; Palacios, J. J.; Kröger, J. Plasticity of single-atom Pb junctions. *Phys. Rev. B* **2016**, *93*, 235402.

(57) Kresse, G.; Furthmüller, J. Efficient Iterative Schemes for Ab Initio Total-Energy Calculations Using a Plane-Wave Basis Set. *Phys. Rev. B* **1996**, *54*, 11169–11186.

(58) Kresse, G.; Furthmüller, J. Efficiency of ab-initio total energy calculations for metals and semiconductors using a plane-wave basis set. *Comput. Mater. Sci.* **1996**, *6*, 15–50.

(59) Kresse, G.; Joubert, D. From ultrasoft pseudopotentials to the projector augmented-wave method. *Phys. Rev. B* **1999**, *59*, 1758–1775.

(60) Klimeš, J.; Bowler, D. R.; Michaelides, A. Chemical accuracy for the van der Waals density functional. *J. Phys.: Condens. Matter* **2010**, *22*, 022201.

(61) Klimeš, J.; Bowler, D. R.; Michaelides, A. Van der Waals density functionals applied to solids. *Phys. Rev. B* **2011**, *83*, 195131.

(62) Beck, P.; Schneider, L.; Rózsa, L.; Palotás, K.; Lászlóffy, A.; Szunyogh, L.; Wiebe, J.; Wiesendanger, R. Spin-orbit coupling induced splitting of Yu-Shiba-Rusinov states in antiferromagnetic dimers. *Nature Communications* **2021**, *12*, 2040.

TOC Graphic